Journal of Alloys and Compounds 509 (2011) L103–L108

Contents lists available at ScienceDirect

Journal of Alloys and Compounds

journal homepage: www.elsevier.com/locate/jallcom

Letter

Structural and magnetic properties of sputter deposited cobalt–silica nanocomposite thin films

Rajan Walia [a], J.C. Pivin [b], A.K. Chawla [a], R. Jayaganthan [c], Ramesh Chandra [a,*]

[a] Nanoscience Laboratory, Institute Instrumentation Centre, Indian Institute of Technology Roorkee, Roorkee 247667, India
[b] Centre Spectrometrie Nucleaire et de Spectrometrie de Masse (CSNSM), IN2P3-CNRS, Batiment 108, 91405 Orsay Campus, France
[c] Department of Metallurgical and Materials Engineering, Indian Institute of Technology Roorkee, Roorkee 247667, India

ARTICLE INFO

Article history:
Received 27 August 2010
Received in revised form
19 November 2010
Accepted 22 November 2010
Available online 1 December 2010

Keywords:
Magnetron sputtering
Nanocomposites
Superparamagnetism
Blocking temperature

ABSTRACT

The present study was focused to investigate the effect of Co concentration on structural and, magnetic properties of Co–SiO_2 nanocomposite thin films. Co–SiO_2 nanocomposite films with different cobalt atomic concentration up to 49 at% were synthesized using direct current (DC) and radiofrequency (RF) magnetron co-sputtering. TEM and XRD analyses reveal the formation of both FCC (1 1 1) and HCP (1 0 1) phases in all the samples. The particle size and surface roughness of these films is found to increase with increase in cobalt concentration. Magnetic measurements reveal that the embedded cobalt nanoparticles behave as superparamagnets when their size is ≤16 nm. The coercivity at 3 K decreases while value of blocking temperature increases with increase in the size of embedded Co nanoparticles.

1. Introduction

Nanocomposite thin films made of transition metal particles embedded in insulating matrix such as Co–SiO_2, Ni–SiO_2, and Fe–SiO_2 exhibit superior magnetic and optical properties, which may be exploited for optoelectronic device applications [1]. The properties of magnetic nanoparticles are different from those of the bulk magnets because, in nanoparticles, an increasing fraction of the magnetic atoms lies at the surface, thus reducing the average number of neighbors and favoring the interaction with the surrounding atoms of the matrix. Below a critical diameter of 10–100 nm (values for typical materials) the magnetic particle supports only one domain. Single domain magnetic particles are attractive for technological applications, such as high coercive films for data storage and giant magnetoresistance for read heads. The interest in nanocomposites consisting of nanometric magnetic particles embedded in an insulating matrix such has silica has grown considerably in recent years due to new magnetic properties presented by these kind of materials. For metal volume fraction well below the percolation limit, the insulating host matrix prevents the interaction among nanoparticles, thus giving an ideal frame to investigate their intrinsic magnetic properties. The magnetic properties of such systems are closely related to the particle size and concentration [2–5]. For example, Sen et al. have recently studied the effect of concentration of Co nanoparticles in SiO_2 matrix [6]. Lu et al. have studied the effect of SiO_2 matrix on the growth of Co nanoparticles [7]. However, from the basic research point of view it would be much more interesting to synthesize such systems in which all the parameters affecting the average magnetic properties, such as particle size and size distribution, crystalline phase, spatial arrangement of nanoparticles, could be varied independently and their effects could be studied. Co nanoparticles below a critical size, show superparamagnetism due to their lower magnetic energy in the form of single domains [3]. Within single domain particle magnetic moments flip all together as a supermoment between easy magnetization axes when thermal energy is larger than the anisotropy energy barrier. Thus the magnetic behavior of an ensemble of this kind of single-domain particles is paramagnetic-like [8–10]. It is well known that paramagnetic nanoparticles are not suitable as memory storage since thermal fluctuations result in losing stored data. Several efforts have been made to stabilize the residual magnetization of nanoparticles under zero applied field, for instance by embedding them in an antiferromagnetic matrix [9]. A shell of CoO or SiO_2 around Co particles could play such a role [11–13]. The studies on magnetic properties of sputter deposited Co–SiO_2 thin films are limited in the literature [14,15]. However study of Co–SiO_2 system synthesized by other techniques like sol–gel and ion implantation has been done by several authors [6–8,16–22]. Therefore, the present

* Corresponding author. Tel.: +91 1332 285743; fax: +91 1332 286303.
E-mail address: ramesfic@iitr.ernet.in (R. Chandra).

0925-8388/$ – see front matter © 2010 Elsevier B.V. All rights reserved.
doi:10.1016/j.jallcom.2010.11.151

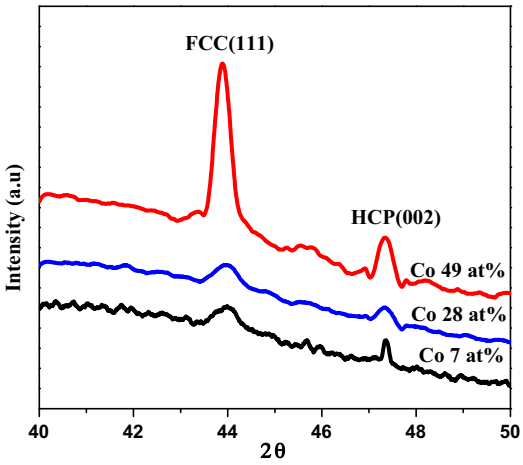

Fig. 1. XRD pattern showing the most intense peaks of FCC and HCP cobalt phases at low angles in samples having different cobalt concentrations.

work is focused on to fabricate Co–SiO_2 nanocomposite films by using DC/RF magnetron co-sputtering and investigate the effect of cobalt concentration on their magnetic behavior. The nanocomposite thin films were characterized by XRD, TEM, AFM, FE-SEM/EDS, and SQUID to substantiate the influence of size effect of Co nanoparticles on their magnetic properties.

2. Experimental

Cobalt–silica nanocomposite films were prepared by co-sputtering of silica and cobalt on Si(1 0 0) substrate by DC/RF magnetron sputtering. Depositions were performed at substrate temperature of 600 °C in Ar atmosphere at a pressure of 20 mTorr. The RF-power to the 2 in. diameter silica target was fixed at 250 W during depositions, while the relative amount of cobalt was changed by varying the DC power (from 10 to 50 W) applied to the 2 in. diameter cobalt target (purity 99.95%). Before deposition, the Si substrates were etched in HF then ultrasonically cleaned in propanol-2. All depositions were carried out in three steps: a first single deposition of silica was made for 5 min (to avoid the diffusion of Co in Si Substrate) followed by the co-deposition of silica and cobalt (60 min duration for all samples). As a final step in the preparation, a single silica deposition was performed for 5 min (to avoid oxidation of cobalt). Nanocomposite films with different concentrations of Co were prepared following the same procedure. The thicknesses of final nanocomposite films were measured by cross sectional FE-SEM (FEI, QUANTA 200F) image. The cobalt concentrations present in the samples were measured by using the EDAX attachment in the FESEM.

X-ray diffraction (XRD) (Bruker AXS, D8 advance model) was used to study crystallinity, phase formation and particle size of the sputter deposited samples. X-ray diffraction patterns were recorded by using Ni-filtered Cu K_α radiation (30 mA, 40 kV) in air at room temperature with step size of 0.02° in a 2θ scattering angle with time taken per step as 0.5 s. Transmission electron microscopy (TEM) investigation was carried out using a TEM (FEI, TECNAI G^2) microscope operated at 200 kV. Selected area electron diffraction (SAED) revealed the nature of crystalline phases present in the samples. The surface morphology and roughness of the thin films were examined by AFM (NT-MDT, Ntegra), operated in semicontact (tapping) mode.

The magnetic properties of the films were studied using a SQUID (Quantum Design, MPMS XL) magnetometer. Field-cooled (FC) and zero-field-cooled (ZFC) measurements were performed on the films in the temperature range of 3–300 K, under a magnetic field of 500 Oe. Hysteresis loops were recorded at room temperature and 3 K, with a magnetic field up to 10 kOe.

3. Results and discussion

XRD diffraction (shown in Fig. 1) shows that two types of cobalt nanoparticles precipitate in all the studied films showing FCC (1 1 1) and HCP (0 0 2) structures. The films contain FCC particles with a mean size of 10, 16 and 29 nm for cobalt concentration of 7, 28 and 49 at%, respectively. Particle size increases with increase in cobalt concentration which may be due to the agglomeration of cobalt particles takes place at higher concentration. Particle sizes were

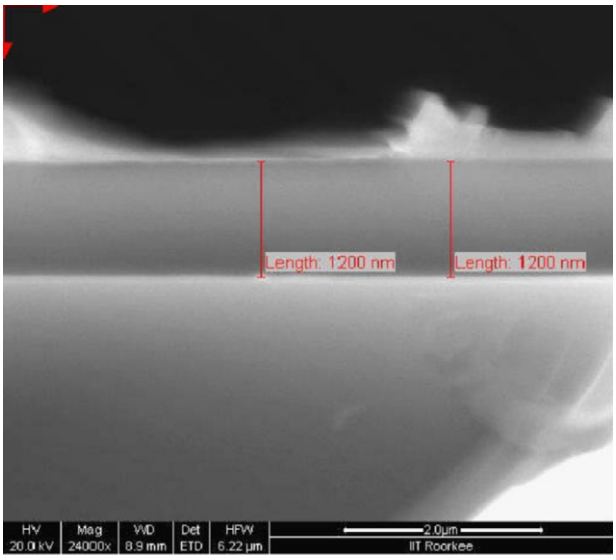

Fig. 2. Cross sectional image of 7 at% Co sample.

calculated by using Scherrer formula [23], given as

$$t = \frac{0.9\lambda}{B\cos\theta}$$

where B is the full-width at half maximum (FWHM) of a Bragg peak in radian, λ is the wavelength of X-ray (1.54 Å for the Cu target), and θ is the Bragg angle.

In our opinion the fact that deserves attention is the simultaneous presence of the FCC and HCP Co phases in the particles studied. In bulk polycrystalline alloys, the HCP Co phase is stable; the polymorphic transition to the FCC phase occurs above 420 °C. Numerous experimental studies, which were aimed at the production and analysis of nanocrystalline Co and Co nanoparticles, demonstrated that FCC Co is stable in these structural modifications at room temperature [24–29]. A study of free Co nanoparticles [25] showed that at room temperature in Co particles $\leq$20 nm in size there is only an FCC phase; in particles of 20–40 nm, a mixture of the FCC and HCP phases is observed; and in Co particles $\geq$40 nm in size, the HCP structure is revealed. Note that the contact of nanoparticles and the matrix material naturally can change the ranges of the particle sizes in which the FCC and HCP phases are stable [30–34]. For example, the HCP phase is stable, along with the FCC phase, in cobalt particles

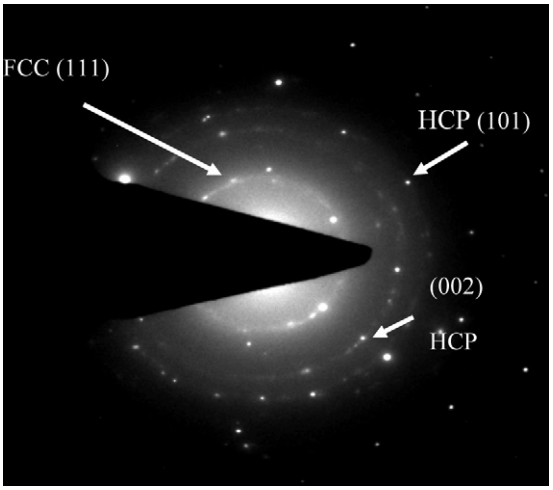

Fig. 3. SAED image of sample having 28 at% Co.

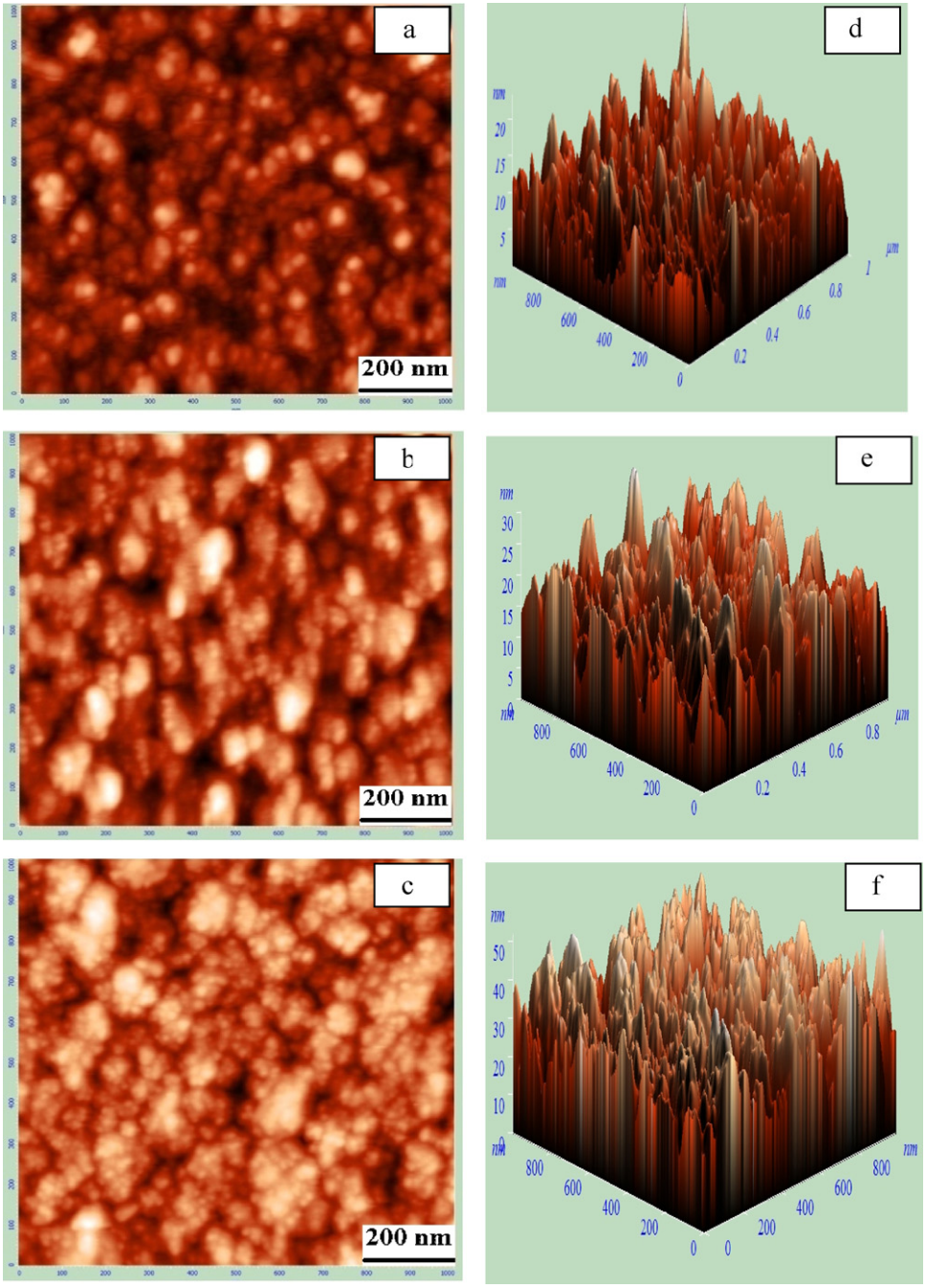

Fig. 4. AFM images for (a) 7 at%, (b) 28 at% and (c) 49 at% showing the increase in density of the material with increase in cobalt concentration and 3D images for (d) 7 at%, (e) 28 at% and (f) 49 at% shows the roughness increase with increase in cobalt concentration.

about 5 nm in size in an ultrafine teflon matrix [34]. The composites used in our study had Co particles of 10–29 nm in size and also contained the FCC and HCP phases simultaneously.

Cobalt concentrations present in the samples were measured by EDAX attachment in FESEM. The variation of cobalt concentration with the power given to cobalt target is given in Table 1. The thicknesses of nanocomposite films were measured by taking their cross sectional image in FESEM (Fig. 2). The measured thicknesses were found to be 1.2, 1.9, and 2.3 μm, for the samples containing 7, 28, and 49 at% cobalt, respectively. The thickness of the films is found to increase with increase in cobalt concentration, for the obvious reason that the total DC power was increased for increasing the Co concentration. In order to observe the spatial distribution of the two FCC and HCP phases in cobalt nanoparticles selected area electron diffraction patterns were taken in the Transmission Electron Microscope. SAED pattern of the sample Co 28 at% (shown in Fig. 3) reveals the formation of FCC (1 1 1) and HCP (1 0 1) and (0 0 2) phases of cobalt nanoparticles in silica matrix. The results obtained

Table 1
Value of coercivities at 3 K and 300 K and blocking temperature for different cobalt concentration in films.

Power given to Co target (W)	Co conc. (at%)	Coercivity (Oe) at 3 K	Coercivity (Oe) at 300 K	Blocking temp (K)
10	7	1505	0	27
25	28	1104	0	70
50	49	376	251	Above 300

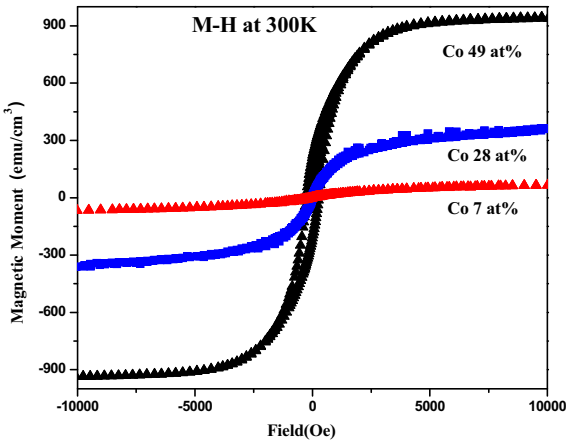

Fig. 5. *M–H* curves of samples having different cobalt concentration at 300 K.

in SAED pattern support the measurements taken by XRD which also shows the formation of both FCC and HCP phases in the samples. The surface topography of the samples was studied by Atomic Force Microscopy. The AFM images (shown in Fig. 4) reveal that the density of the films increases with increase in Co concentration. While the root mean square (rms) value of roughness is found to be 1.56, 4.45 and 7.22 nm for 7, 28 and 49 at% Co samples, respectively.

The magnetic behavior of the nanocomposite films was investigated by measuring the hysteresis loops at 300 K and 3 K by SQUID Magnetometer as shown in Figs. 5 and 6, respectively. For all the samples, the measured magnetic moments were normalized to volume of the respective films. It is observed that the film containing 49% Co remains is ferromagnetic up to room temperature (RT) while less concentrated systems show no more residual magnetization at RT which may be signature of superparamagnetism. In Fig. 7(a) variation of coericivity at room temperature for different samples having different cobalt concentration has been plotted. Looking at the hysteresis loops at 3 K (Fig. 6) for these samples we find that the coercivity (given in Table 1) found to decrease with increase in the cobalt concentration which could be due to the fact that increase in cobalt concentration leads to increase in particle size that results in the transformation of particles from single domain (for Co 7 at%) to multi-domain (in case of Co 28 at% and Co 49 at%).

The magnetization of a multi-domain particle can be changed (in presence of external field) by moving the position of a domain wall, which causes some domains to increase in size and others to decrease. A multi-domain particle may contain many easily mov-

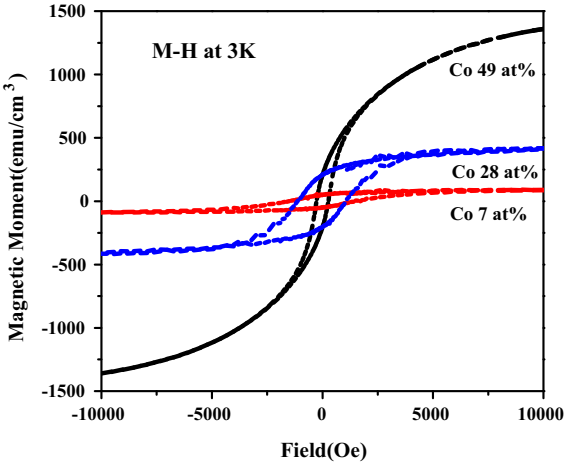

Fig. 6. *M–H* curves of samples having different cobalt concentration at 3 K.

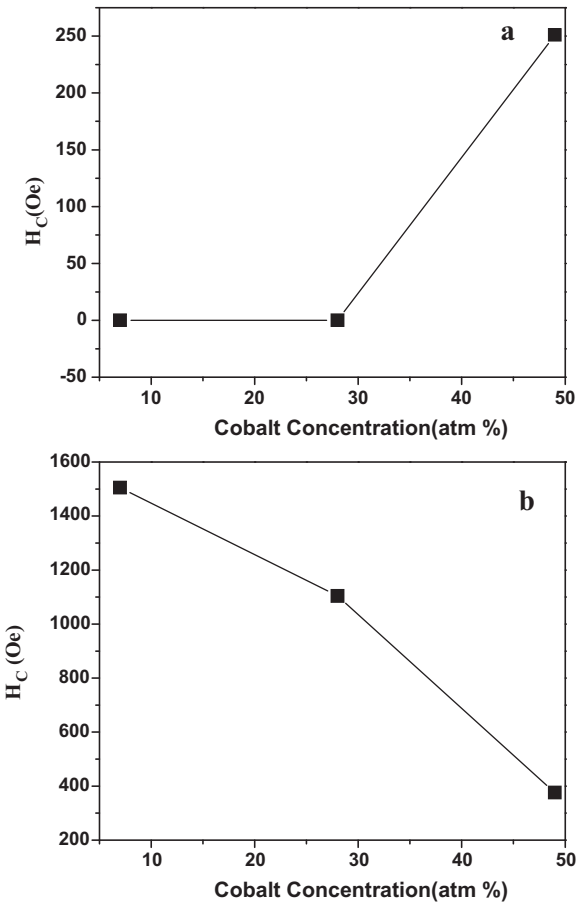

Fig. 7. Variation of H_c at 3 K (a) and 300 K (b) with different cobalt concentration.

able domain walls. Consequently, it is much easier to change the magnetization of a multi-domain particle than of a single domain particle. As a result multi-domain particles are less stable carriers of remanent magnetization than single domain particles. Therefore multi-domain particles have less coercivity than single domain particles. The coercivity behavior of multidomain particles is found to be according to the following relation:

$$H_c = a + \frac{b}{D}$$

where H_c is coercivity, 'a' and 'b' are constants and 'D' is the diameter of the particle [35]. It is clear from this relation that coercivity for multidomain particles decreases with increase in particle size. Coercivities at 3 K for different cobalt concentration has been plotted in Fig. 7(b) which shows the decrease in coercivity values with increase in cobalt concentration.

In the studied samples both HCP and FCC phase of cobalt particles are present. HCP-Co is magnetically harder than the FCC phase due to its magnetic anisotropy and high coercivity as compared to the symmetrical and low coercivity FCC phase. Because of the difference in crystal structure, variations in physical and magnetic properties between the two polymorphs arise. HCP-Co is slightly denser than FCC-Co, even though both phases are close-packed structures. Thus; the highly anisotropic HCP-Co is more desirable for magnetic recording and other permanent magnet applications [36,37]. On the other hand, the FCC phase is more suitable for soft magnetic applications [38]. In our samples both the phases are present. Presence of highly anisotropic HCP phase may be one of the reasons of high coercivity obtained in our samples.

Composite films formed of isolated nanograins exhibit magnetic features dominated by their thermal demagnetization (superpara-

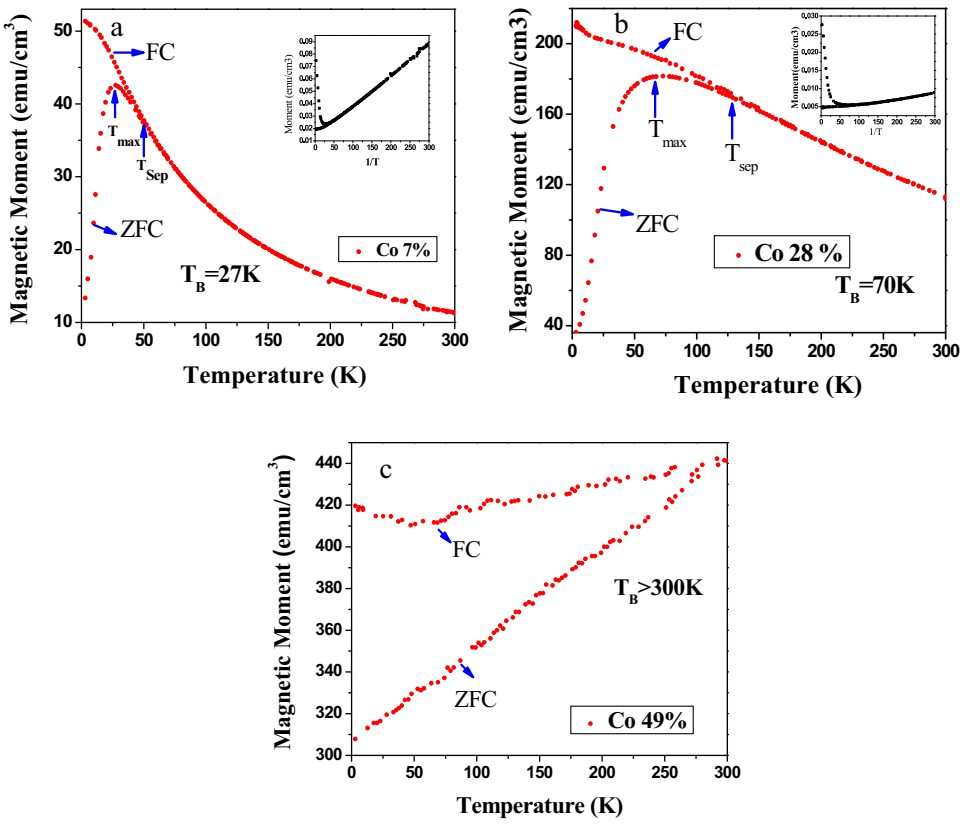

Fig. 8. FC–ZFC curves of samples having different cobalt concentration (a) 7 at%, (b) 28 at% and (c) 49 at%.

magnetic behavior) above the temperature at which the thermal energy becomes larger than the magnetic energy barrier. This threshold temperature T_B, called blocking temperature, above which a particle with volume V and magnetic anisotropy energy per unit volume K_{eff} (generally of crystalline origin) exhibits the superparamagnetic behavior, is expressed by the following equation

$$T_B = \frac{K_{eff} V}{\alpha k_B} \quad (1)$$

where k_B is the Boltzmann constant, and α is a constant usually taken as 25 in the case of SQUID measurements [14]. The superparamagnetic behavior of the nanocomposite films was investigated by using the zero-field cooled (ZFC) and field cooled (FC) procedure to observe a maximum of magnetization close to T_B and a Curie law above T_B. Magnetization measurements versus 'T' under a field of 500 Oe are shown in Fig. 8.

At high temperature (Fig. 8) both the FC and ZFC curves coincide and their behavior approximately follows a Curie–Weiss law (which is evident from the plot of 'M' verses '$1/T$' shown in the insets of Fig. 8(a) and (b)). At low temperatures, the ZFC and FC curves separate and the ZFC magnetization curve exhibits a broad maximum, characteristic of superparamagnetism. It occurs due to the progressive de-blocking of particles of increasing size when the temperature is increased. The maximum temperature in the ZFC curve (T_{max}) is related to the blocking of particles with mean size, while the temperature at which the ZFC and FC curves begin to separate (T_{sep}) corresponds to the blocking of the largest particles. The average blocking temperature of the sample is defined by the blocking temperature of particles with mean size. Thus the blocking temperatures for cobalt concentrations of 28 at% and 7 at% are 70 K and 27 K, respectively. The particles size calculated from corresponding T_B values (using Eq. (1)) are found to be 7 nm and 5 nm for 28 at% cobalt and 7 at% cobalt, respectively. The observed difference from the particle sizes calculated by XRD peaks may be because of the fact that we got too high value of T_B which may be because of (i) particles dipoles interaction or (ii) their anisotropy energy is increased by stress [39–41]. The value of magnetic anisotropy used in calculation of particle sizes from T_B is $6.3 \times 10^5\,\mathrm{J\,M^{-3}}$ [42]. In 7 at% Co nanocomposite thin films, the separation of the ZFC–FC is increasing at low temperatures, which reveals that the nanoparticles are mainly blocked, in agreement with the hysteresis measurements. With increase in temperature, the ZFC curves exhibit a maximum; it is an indication of the progressive transformation of nanoparticles to superparamagnetic behavior. All the nanoparticles show superparamagnetic behavior above the temperature at which the ZFC–FC branches combine. It is evident that the nanocomposite films with Co concentration of 28 at%, and 7 at% samples are superparamagnetic at 300 K, and also from the zero value of coercive field at room temperature as shown in Fig. 6. For the nanocomposite films with 7 at% Co, relatively small broadening of the ZFC curve is observed and the fact that T_{sep} and T_{max} are quite close to each other suggests a narrow size distribution of the Co particles. While the observed ZFC–FC curves for the Co 28 at% sample shows larger separation between T_{sep} and T_{max} and the effects of both particle size and magnetic anisotropy distributions [14].

4. Conclusions

The Co–SiO_2 nanocomposite films were deposited by using DC/RF magnetron co-sputtering. The XRD results showed the formation of FCC + HCP structure in the films deposited with 7, 28 and 49 at% Co concentration. The AFM results show increase in roughness with increase in cobalt concentration. It is observed that the magnetic properties of Co–SiO_2 nanocomposite films are influenced by size, composition, and surface properties of the Co nanoparticles. ZFC–FC curves show the signature of superparamag-

netism ≤16 nm size of Co nanoparticles. SAED pattern of the films shows the formation of both HCP and FCC structures, which are in agreement with the XRD results. It is evident from the ZFC–FC curves that blocking temperature increases with increase in particle size. Value of coercivity is found to decrease with increase in particle size.

Acknowledgements

One of the authors, Rajan Walia is thankful to AICTE (All India Council for Technical Education) for awarding fellowship for this work.

References

[1] E. Cattaruzza, G. Battaglin, F. Gonella, R. Polloni, G. Mattei, C. Maurizio, P. Mazzoldi, C. Sada, M. Montagna, C. Tosello, M. Ferrari, Philos. Mag. B 82 (2002) 735–744.
[2] P.A. Kumar, S. Mitra, K. Mandal, Indian J. Pure Appl. Phys. 45 (2007) 21–26.
[3] L.G. Jacobsohn, J.D. Thompson, R.M. Dickerson, M. Nastasi, Nucl. Instrum. Methods B 257 (2007) 447–450.
[4] N.S. Gajbhiye, S. Sharma, A.K. Nigam, R.S. Ningthoujam, Chem. Phys. Lett. 466 (2008) 181–185.
[5] F. Mazaleyrat, M. Ammar, M. LoBue, J.-P. Bonnet, P. Audebert, G.-Y. Wang, Y. Champion, M. Hÿtch, E. Snoeck, J. Alloys Compd. 483 (2009) 473–478.
[6] R. Sen, G.C. Das, S. Mukherjee, J. Alloys Compd. 490 (2010) 515–523.
[7] X. Lu, L. Giang, Q. Sun, C. Yang, J. Solid State Chem. 183 (2010) 1555–1560.
[8] E. Cattaruzza, F. Gonella, G. Mattei, P. Mazzoldi, D. Gatteschi, C. Sangregorio, M. Falconieri, G. Salvetti, G. Battaglin, Appl. Phys. Lett. 73 (1998) 1176–1178.
[9] M. Respaud, J.M. Broto, H. Rakoto, A.R. Fert, L. Thomas, B. Barbara, M. Verelst, E. Snoeck, P. Lecante, A. Mosset, J. Osuna, T. Ould Ely, C. Amiens, B. Chaudret, Phys. Rev. B 57 (1998) 2925–2935.
[10] F. Luis, J.M. Torres, L.M. García, J. Bartolomé, J. Stankiewicz, F. Petroff, F. Fettar, J.L. Maurice, A. Vaurès, Phys. Rev. B 65 (2002) 094409.
[11] V. Skumryev, S. Stoyanov, Y. Zhang, G. Hadjipanayis, D. Givord, Josep Nogué, Nature 423 (2003) 850–853.
[12] X. Yan, G. Chai, D. Xue, J. Alloys Compd. 509 (2010) 1310–1313.
[13] X.J. Yina, K. Peng, A.P. Hua, L.P. Zhoua, J.H. Chen, Y.W. Du, J. Alloys Compd. 479 (2009) 372–375.
[14] E. Cattaruzza, G. Battaglin, P. Canton, C. de Julián Fernández, M. Ferroni, F. Gonella, C. Maurizio, P. Riello, C. Sada, C. Sangregorio, B.F. Scremin, Appl. Surf. Sci. 226 (2004) 62–67.
[15] E. Cattaruzza, G. Battaglin, P. Canton, C. de Julián Fernández, M. Ferroni, T. Finotto, C. Maurizio, C. Sada, J. Non-Cryst. Solids 336 (2004) 148–152.
[16] G. Ennas, G. Marongiu, S. Marras, G. Piccaluga, J. Nanopart. Res. 6 (2004) 99–105.
[17] C. Maurizio, G. Mattei, P. Canton, E. Cattaruzza, C. de Julián Fernández, P. Mazzoldi, F. D'Acapito, G. Battaglin, C. Scian, A. Vomiero, Mater. Sci. Eng. C 27 (2007) 193–196.
[18] G. Mattei, C. Maurizio, C. de Julián Fernández, P. Mazzoldi, G. Battaglin, P. Canton, E. Cattaruzza, C. Scian, Nucl. Instrum. Methods B 250 (2006) 206–209.
[19] E. Cattaruzza, G. Battaglin, P. Canton, C. Sada, J. Non-Cryst. Solids 351 (2005) 1932–1936.
[20] P. Gangopadhyay, T.R. Ravindran, K.G.M. Nair, S. Kalavathi, B. Sundaravel, B.K. Panigrahi, Appl. Phys. Lett. 90 (2007) 063108.
[21] S.M. Park, W. Ki, J. Yu, H. Du, J. Mater. Res. 20 (2005) 3094–3101.
[22] P. Gangopadhyay, T.R. Ravindran, B. Sundaravel, K.G.M. Nair, B.K. Panigrahi, Nucl. Instrum. Methods B 266 (2008) 1647–1652.
[23] B.D. Cullity, Elements of X-ray Diffraction, 2nd ed., Addison Wesley, London, 1978, p. 102.
[24] S.P. Gubin, Yu.A. Koksharov, Neorg. Mater. 38 (2002) 287–1305.
[25] O. Kitakami, H. Sato, Y. Shimada, F. Sato, M. Tanaka, Phys. Rev. B 56 (1997) 13849–13854.
[26] J. Jun, S. Supapan, X. Wang, J.C. Withers, J. Appl. Phys. 80 (1996) 103–108.
[27] W. Wernsdorfera, C. Thirion, N. Demoncy, H. Pascard, D. Mailly, J. Magn. Magn. Mater. 242–245 (242) (2002) 132–138.
[28] R.S. Iskhakov, S.V. Stolyar, L.A. Chekanova, E.M. Artem'ev, V.S. Zhigalo, JETP Lett. 72 (2000) 316–319.
[29] S.V. Komogortsev, R.S. Iskhakov, K.A. Shaikhutdinov, V.K. Mal'tsev, A.V. Okotrub, A.G. Kudashov, U.V. Shubin, Phys. Met. Metallogr. 102 (2006) S67–S70.
[30] T. Hinotsu, B. Jeyadevan, C.N. Chinnasamy, K. Shinoda, K. Tohji, J. Appl. Phys. 95 (2004) 7477–7479.
[31] R.H. Kodama, A.S. Edelstein, J. Appl. Phys. 85 (1999) 4316–4318.
[32] Y. Bao, M. Beerman, K.M. Krishnan, J. Magn. Magn. Mater. 266 (2003) L245–L249.
[33] G.H. Lee, S.H. Huh, J.W. Jeong, H.-C. Ri, J. Magn. Magn. Mater. 246 (2002) 404–411.
[34] V.V. Matveev, D.A. Baranov, G.Y. Yurkov, N.G. Akatiev, I.P. Dotsenko, S.P. Gubin, Chem. Phys. Lett. 422 (2006) 402–405.
[35] B.D. Cullity, C.D. Graham, Introduction to Magnetic Materials, 2nd ed., John Wiley & Sons, New Jersey, 2009, 361 pp.
[36] P. Gambardella, S. Rusponi, M. Veronese, S.S. Dhesi, C. Grazioli, A. Dallmeyer, I. Cabria, R. Zeller, P.H. Dederichs, K. Kern, C. Carbone, H. Brune, Science 300 (2003) 1130–1133.
[37] S. Rusponi, T. Cren, N. Weiss, M. Epple, L. Claude, P. Buluschek, H. Brune, Nat. Mater. 2 (2003) 546–551.
[38] D.P. Dinega, M.G. Bawendi, Angew. Chem. Int. Ed. 38 (1999) 1788–1791.
[39] J.L. Dormann, F. D'Orazio, F. Lucari, E. Tronc, P. Prené, J.P. Jolivet, D. Fiorani, R. Cherkaoui, M. Noguès, Phys. Rev. B 53 (1996) 14291–14297.
[40] G. Suran, A. Stankoff, F. Hoffmann, Phys. Rev. B 8 (1973) 1109–1118.
[41] J.P. Chen, C.M. Sorensen, K.J. Klabunde, G.C. Hadjipanayis, Phys. Rev. B 51 (1995) 11527–11532.
[42] H.P. Oepen, M. Benning, H. Ibach, C.M. Schneider, J. Kirschner, J. Magn. Magn. Mater. 86 (1990) L137–L142.